# Electronic Supplementary Information (†ESI)

## Tailoring copper valence states in $CuO_\delta/\gamma$-$Al_2O_3$ catalysts by an *in situ* technique induced superior catalytic performance for simultaneous elimination of NO and CO

**Xiaojiang Yao,[ab] Fei Gao,[b] Yuan Cao,[ab] Changjin Tang,[*ab] Yu Deng,[b] Lin Dong[*ab] and Yi Chen[ab]**

[a] *Key Laboratory of Mesoscopic Chemistry of MOE, School of Chemistry and Chemical Engineering, Nanjing University, Nanjing 210093, China. E-mail: tangcj@nju.edu.cn; donglin@nju.edu.cn*

[b] *Jiangsu Key Laboratory of Vehicle Emissions Control, Center of Modern Analysis, Nanjing University, Nanjing 210093, China.*

## Experimental section

**Catalysts preparation.** A kind of commercial γ-$Al_2O_3$ powder was purchased from Fushun Petrochemical Institute in China, and used as carrier to prepare supported copper-based catalysts in this study. Before the introduction of copper species, the carrier was calcined at 750 °C for 7 h in the flowing air, and its Brunauer-Emmett-Teller (BET) specific surface area was 134.1 $m^2$ $g^{-1}$.

CuO/γ-$Al_2O_3$ catalysts were prepared by wet impregnation of γ-$Al_2O_3$ with an aqueous solution containing a required amount of $Cu(NO_3)_2 \cdot 3H_2O$. The samples were dried at 110 °C overnight, and then calcined at 500 °C for 5 h in the flowing air. For simplicity, the resultant catalysts are denoted as *x*CuAl, *e.g.,* 06CuAl corresponds to the catalyst with a copper oxide loading amount of 0.6 mmol $Cu^{2+}$/100 $m^2$ γ-$Al_2O_3$.

Cu/γ-$Al_2O_3$ catalysts were obtained through reducing the corresponding CuO/γ-$Al_2O_3$ catalysts by $H_2$. Before switching to $H_2$, all the samples were pretreated in a flowing high purified $N_2$ stream at 350 °C for 1 h. After that, the samples were exposed to $H_2$-Ar mixture (7.0% $H_2$ by volume) at a rate of 70 mL $min^{-1}$, and held for 1 h at 350 °C. The choice of the reduced pretreatment temperature is according to the $H_2$-TPR results that these CuO/γ-$Al_2O_3$ catalysts can be fully reduced at this temperature. The reduced samples were cooled to ambient temperature in the flowing high purified $N_2$. The resultant catalysts are denoted as *x*CuAl-R, *e.g.,* 06CuAl-R corresponds to the catalyst with a copper oxide loading amount of 0.6 mmol $Cu^{2+}$/100 $m^2$ γ-$Al_2O_3$ following a reduced pretreatment to get $Cu^0$ species.

$Cu_2O$/γ-$Al_2O_3$ catalysts were acquired through reducing and re-oxidizing the

corresponding CuO/γ-$Al_2O_3$ catalysts by $H_2$ and $N_2O$. In the first stage, reducing CuO/γ-$Al_2O_3$ catalysts by $H_2$ to obtain Cu/γ-$Al_2O_3$ catalysts, which is similar with the procedure of *x*CuAl-R catalysts. In the previous works, many researchers reported that $N_2O$ could be dissociatively adsorbed on the surface of metallic Cu, and oxidize its surface to generate $Cu_2O$ at 50 °C.[S1-S3] Therefore, in the second stage, re-oxidizing Cu/γ-$Al_2O_3$ catalysts *via* $N_2O$ to get $Cu_2O$/γ-$Al_2O_3$ catalysts. Before switching to $N_2O$, all the samples were heated to 50 °C with a ramp of 10 °C $min^{-1}$ in a flowing high purified $N_2$ stream. After that, the samples were exposed to $N_2O$-$N_2$ mixture (20.0% $N_2O$ by volume) at a rate of 70 mL $min^{-1}$, and held for 1 h at 50 °C. The re-oxidized samples were cooled to ambient temperature in the flowing high purified $N_2$. The resultant catalysts are denoted as *x*CuAl-RO, *e.g.*, 06CuAl-RO corresponds to the catalyst with a copper oxide loading amount of 0.6 mmol $Cu^{2+}$/100 $m^2$ γ-$Al_2O_3$ following the reduced and re-oxidized pretreatment to obtain surface $Cu^+$ species.

**Catalysts characterization**

The Brunauer-Emmett-Teller (BET) specific surface area of γ-$Al_2O_3$ was measured by nitrogen physisorption at 77 K using a Micromeritics ASAP-2020 analyzer. Prior to the analysis, the sample was degassed under vacuum at 300 °C for 4 h.

X-ray diffraction (XRD) patterns of the *in situ* pretreated catalysts were recorded on a Philips X'pert Pro diffractometer using Ni-filtered Cu Kα radiation (λ = 0.15418 nm), which is equipped with a reaction chamber. The *in situ* pretreatment was carried out in the reaction chamber. Furthermore, the X-ray tube was operated at 40 kV and

40 mA.

$H_2$-temperature programmed reduction ($H_2$-TPR) experiments of these catalysts were performed in a quartz U-type reactor connected to a thermal conductivity detector (TCD) with Ar-$H_2$ mixture (7.0% of $H_2$ by volume, 70 mL $min^{-1}$) as a reductant. The *in situ* pretreatment was carried out in the same quartz U-type reactor. Prior to the reduction, the sample (50 mg) was pretreated in a high purified $N_2$ stream at 350 °C for 1 h and then cooled to room temperature. After that, the TPR profiles were collected from 50 °C to target temperature at a rate of 10 °C $min^{-1}$.

X-ray photoelectron spectroscopy (XPS) and X-ray Auger electron spectroscopy (XAES) measurements of the *in situ* pretreated catalysts were performed on a PHI 5000 VersaProbe system, using monochromatic Al Kα radiation (1486.6 eV) operating at an accelerating power of 15 kW. The instrument used in this study has three chambers, namely (1) an ultra high vacuum (UHV) surface analysis chamber; (2) a sample transfer antechamber; and (3) a reaction chamber. The transfer antechamber is connected to both the analysis and reaction chamber. The *in situ* pretreatment was carried out in the reaction chamber. Before the measurement, the sample was further outgassed at room temperature in the UHV chamber ($< 5 \times 10^{-7}$ Pa). The sample charging effects were compensated by calibrating all binding energies (BE) with the adventitious C 1s peak at 284.6 eV. This BE values gave an accuracy at ±0.1 eV.

NO-temperature programmed desorption (NO-TPD) measurements of these catalysts were carried out using a quartz reactor connected to a quadrupole mass spectrometer (Agilent 5975C). The *in situ* pretreatment was carried out in the same

quartz reactor. Prior to the adsorption, the catalyst (100 mg) was pretreated in a flowing high purified He stream (30 mL $min^{-1}$) at 500 °C for 1 h to ensure that all the carbonates on the surface of the catalyst were dissociated, and then cooled to room temperature. After that, the adsorption was performed by using NO-He (5.0% of NO by volume, 30 mL $min^{-1}$) as the adsorbate gas at room temperature for 1 h. The catalyst was further exposed to a high purified He stream (30 mL $min^{-1}$) for 1 h at room temperature to remove all the physically adsorbed NO species. Finally, the TPD measurement started from room temperature to target temperature in a high purified He stream (30 mL $min^{-1}$) at a rate of 10 °C $min^{-1}$.

*In situ* Fourier transform infrared (*in situ* FT-IR) spectra of these catalysts were collected from 400 to 4000 $cm^{-1}$ at a spectral resolution of 4 $cm^{-1}$ (number of scans, 32) on a Nicolet 5700 FT-IR spectrometer equipped with a DTGS as detector. The sample was pressed into a self-supporting wafer (about 10 mg), and mounted in a commercial controlled environment chamber. The *in situ* pretreatment was carried out in the same chamber. The wafer was pretreated with high purified $N_2$ at 350 ºC for 1 h. After cooling to room temperature, the sample was exposed to a controlled stream of CO-Ar (5% of CO by volume) and NO-Ar (5% of NO by volume) at a rate of 10.0 ml·$min^{-1}$ for 1 h to be saturated. NO and CO co-adsorption *in situ* FT-IR spectra were recorded at various target temperatures at a rate of 10 °C·$min^{-1}$ from room temperature to 300 ºC by subtraction of the corresponding background reference (collected from the gas data at each target temperature without the sample).

**Catalytic performance test**

The catalytic performance of these catalysts for NO reduction by CO was evaluated under steady state, involving a feed steam with a fixed composition, 5% NO, 5% CO and 90% He by volume as diluents. The sample (50 mg) was fitted in a fixed bed with a quartz reactor (length, 30 cm; inner diameter, 4 mm; housed in a furnace) and pretreated in a high purified $N_2$ stream at 350 °C for 1 h and then cooled to room temperature, after that, the mixed gases were switched on. The *in situ* pretreatment was carried out in the same quartz reactor. The reaction was taken place at different temperature (the reaction temperature was measured by a K-type thermocouple inserted in the middle of the catalyst bed) with a space velocity of 12,000 $h^{-1}$. Two columns (length, 1.75 m; diameter, 3 mm) and two thermal conductivity detectors (*T* = 100 °C) were used for analyzing the products. Column A filled with Paropak Q for separating $CO_2$ and $N_2O$, column B packed with 5A and 13X molecule sieve (40-60 M) for separating $N_2$, NO and CO. Basically, values of percentage conversion and selectivity in the reaction of NO reduction by CO are defined as:

$$X_{NO}(\%) = \frac{C_{NO}^{in} - C_{NO}^{out}}{C_{NO}^{in}} \times 100, \quad X_{CO}(\%) = \frac{C_{CO}^{in} - C_{CO}^{out}}{C_{CO}^{in}} \times 100, \quad S_{N_2}(\%) = \frac{2C_{N_2}^{out}}{C_{NO}^{in} - C_{NO}^{out}} \times 100$$

Where *X* and *S* are percentage conversion and selectivity, and *C* is the inlet or outlet concentration of the indicated gas.

## Results section

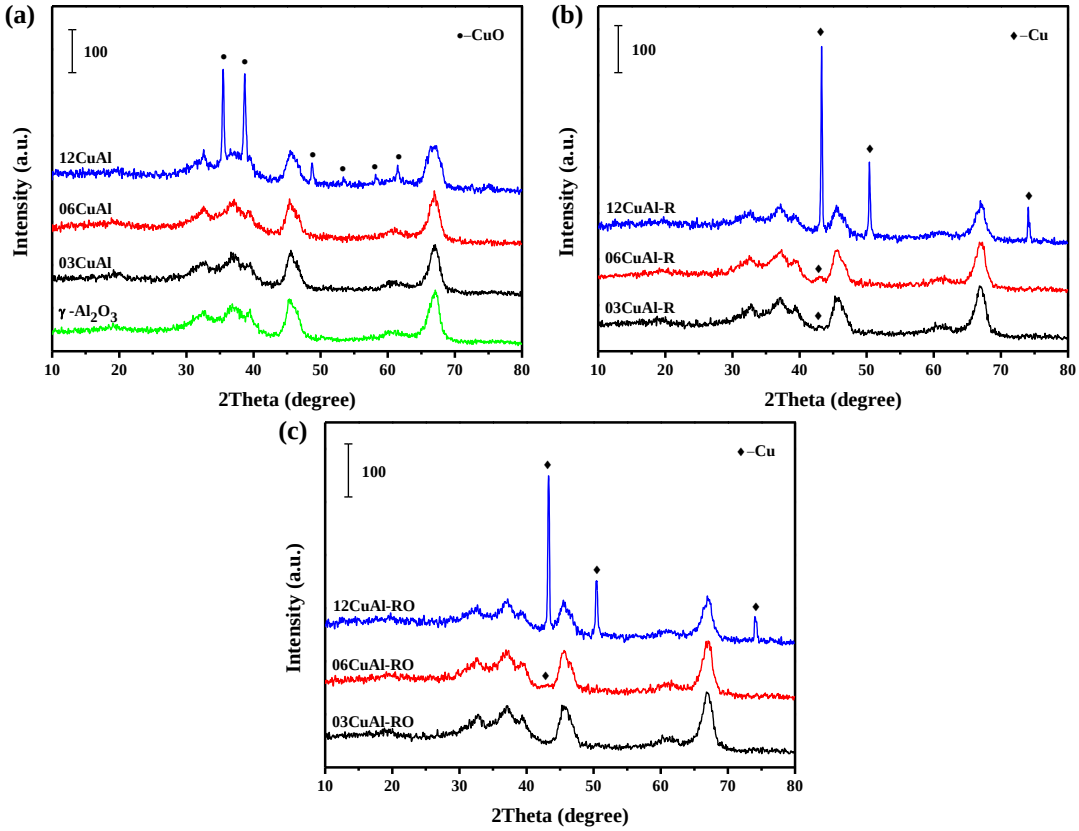


**Fig. S1** XRD patterns of these *x*CuAl catalysts with different pretreatment: (a) fresh samples, (b) reduced samples, and (c) re-oxidized samples.

XRD patterns of these *x*CuAl catalysts with different pretreatment are shown in Fig. S1. For the fresh samples (Fig. S1a), only the characteristic diffraction peaks attributed to γ-$Al_2O_3$ are observed without crystalline CuO in the patterns of 03CuAl and 06CuAl catalysts, while several new characteristic diffraction peaks associated with CuO [PDF-ICDD 48-1548] appear in the pattern of 12CuAl catalyst, indicating that copper oxide species are in the forms of highly dispersed state or/and clustered state on the surface of γ-$Al_2O_3$ when the loading amount is not higher than 0.6 mmol $Cu^{2+}$/100 $m^2$ γ-$Al_2O_3$.[S4] With regard to the reduced samples (Fig. S1b), a weak characteristic diffraction peak corresponding to metallic Cu (111) plane appears at

43.2 ° [PDF-ICDD 04-0836] in the patterns of 03CuAl-R and 06CuAl-R catalysts, and the latter is slightly stronger than the former.[S5] In addition, the characteristic diffraction peaks of crystalline CuO disappear completely, instead, several strong characteristic diffraction peaks of metallic Cu appear in the pattern of 12CuAl-R catalyst. These results suggest that all the highly dispersed copper oxide, clustered CuO, and crystalline CuO on the surface of γ-$Al_2O_3$ can be reduced to crystalline metallic Cu by $H_2$, and the crystallite size of the obtained metallic Cu increases with the increase of copper oxide loading amount. In view of the re-oxidized samples (Fig. S1c), we can find that the characteristic diffraction peak of metallic Cu becomes quite weak even not to be seen in the patterns of 03CuAl-RO and 06CuAl-RO catalysts, the intensity of metallic Cu characteristic diffraction peaks is also weakened obviously in the pattern of 12CuAl-RO catalyst owing to the oxidation of the metallic Cu surface by $N_2O$ to form highly dispersed $Cu_2O$.[S1-S3]

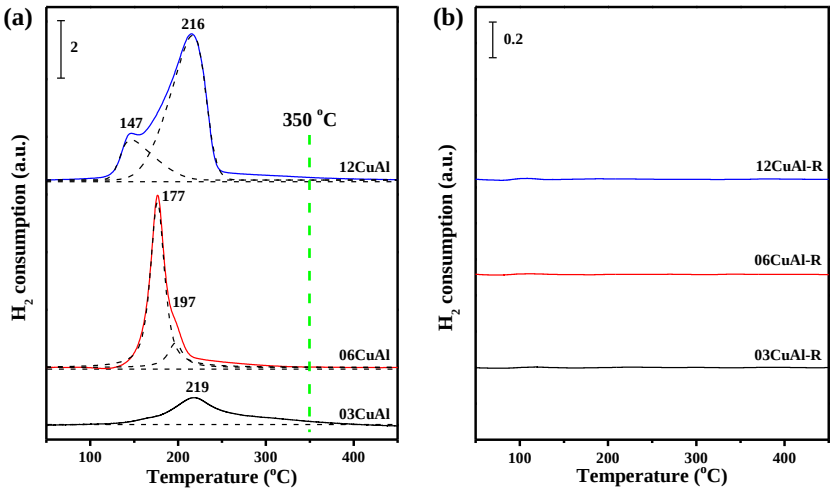

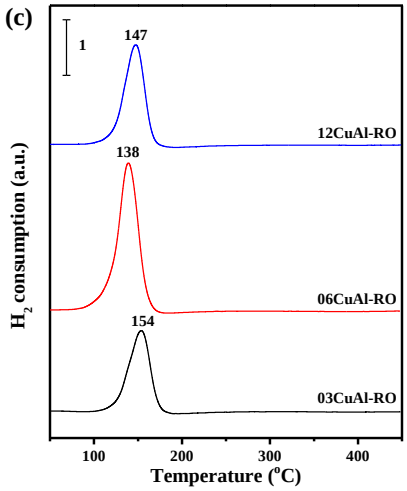


**Fig. S2** $H_2$-TPR profiles of these *x*CuAl catalysts with different pretreatment: (a) fresh samples, (b) reduced samples, and (c) re-oxidized samples.

**Table S1** The quantitative analysis data of $H_2$-TPR over these *x*CuAl catalysts with different pretreatment.

| Catalysts | The actual $H_2$ consumption (μmol/g) | The theoretical $H_2$ consumption (μmol/g) | Cu dispersion degree (%)[a] |
|---|---|---|---|
| 03CuAl | 388.4 | 389.5 | --[b] |
| 06CuAl | 752.2 | 755.4 | -- |
| 12CuAl | 1419.4 | 1424.7 | -- |
| 03CuAl-R | 0 | 0 | 99.02 |
| 06CuAl-R | 0 | 0 | 83.28 |
| 12CuAl-R | 0 | 0 | 32.04 |
| 03CuAl-RO | 192.3 | 194.2 | -- |
| 06CuAl-RO | 313.2 | 376.1 | -- |
| 12CuAl-RO | 227.4 | 709.7 | -- |

[a] The dispersion degree (D) of copper in these *x*CuAl-R catalysts can be calculated from the formula: $D = (2Y/X)\times100\%$, in which X is the actual $H_2$ consumption of fresh *x*CuAl catalysts, Y is the actual $H_2$ consumption of corresponding *x*CuAl-RO catalysts, according to the literatures.[S1-S3] [b] No physicochemical significance.

$H_2$-TPR profiles of these *x*CuAl catalysts with different pretreatment are displayed in Fig. S2. For the fresh samples (Fig. S2a), 03CuAl catalyst exhibits a broad reduction peak at 219 °C attributed to the reduction of highly dispersed CuO.

With the increase of copper oxide loading amount, a strong reduction peak and a shoulder appear at 177 and 197 °C in the $H_2$-TPR profile of 06CuAl catalyst, which are assigned to the reduction of highly dispersed CuO and clustered CuO, respectively. Interestingly, a weak and a strong reduction peaks can be observed at 147 and 216 °C in the $H_2$-TPR profile of 12CuAl catalyst, the former is associated with the reduction of highly dispersed CuO, and the latter is related to the reduction of clustered CuO and crystalline CuO. The obtained results are in good agreement with the XRD results. The quantitative analysis data (Table S1) show that the actual $H_2$ consumption of these *x*CuAl catalysts is close to the corresponding theoretical $H_2$ consumption calculated from $Cu^{2+}$, indicating that the valence state of copper is +2 in these *x*CuAl catalysts. Furthermore, we can find that all the *x*CuAl catalysts can be completely reduced by $H_2$ at 350 °C, which is the basis for the choice of the reduced pretreatment temperature in the present work. With regard to the reduced samples (Fig. S2b), no reduction peaks can be detected in the $H_2$-TPR profiles of these *x*CuAl-R catalysts, suggesting that the valence state of copper is 0 in these *x*CuAl-R catalysts. In view of the re-oxidized samples (Fig. S2c), a single reduction peak can be observed at 154, 138, and 147 °C in the $H_2$-TPR profiles of 03CuAl-RO, 06CuAl-RO, and 12CuAl-RO catalysts, which is attributed to the reduction of surface highly dispersed $Cu_2O$.[S1-S3] In addition, it can be seen from Table S1 that the actual $H_2$ consumption of 03CuAl-RO, 06CuAl-RO, and 12CuAl-RO catalysts is 192.3, 313.2, and 227.4 μmol $g^{-1}$, respectively. However, the corresponding theoretical $H_2$ consumption calculated from $Cu^+$ is 194.2, 376.1, and 709.7 μmol $g^{-1}$. These experimental results and the previous

literatures demonstrate that the valence state of copper is +1 in these *x*CuAl-RO catalysts, and the dispersion degree of copper in the *x*CuAl-R catalysts decreases with the increase of copper oxide loading amount.[S1-S3]

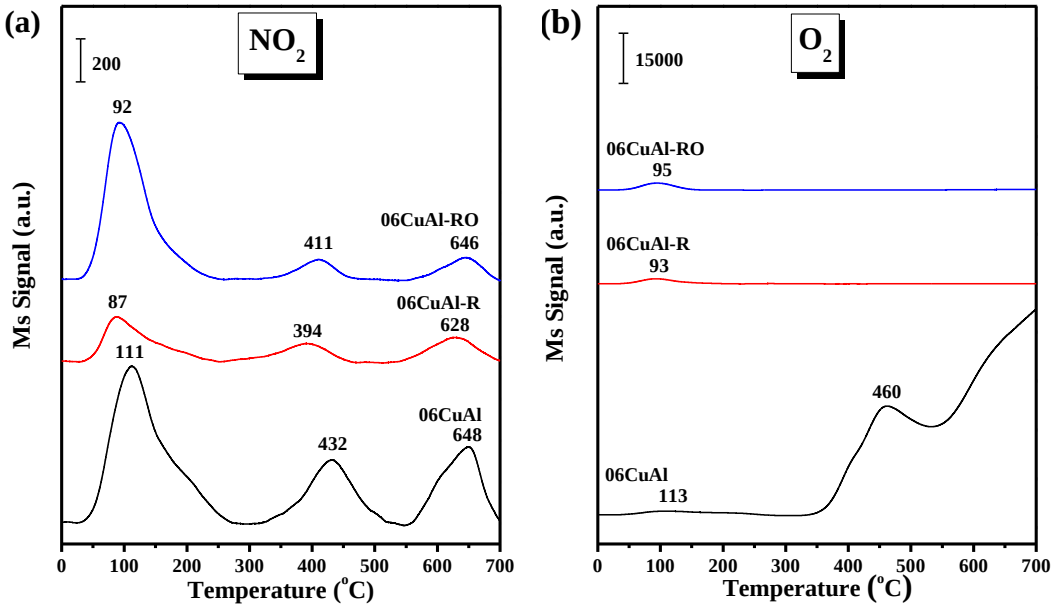


**Fig. S3** NO-TPD profiles: (a) $NO_2$ fragment and (b) $O_2$ fragment over 06CuAl catalysts with different valence states as a function of desorption temperature.

**Table S2** NO-TPD peak area of corresponding fragments over 06CuAl catalysts with different valence states.

| Catalysts | NO peak area (a.u.) | $N_2O$ peak area (a.u.) | $N_2$ peak area (a.u.) | $NO_2$ peak area (a.u.) | $O_2$ peak area (a.u.) |
|---|---|---|---|---|---|
| 06CuAl | $8.19094\times10^7$ | $0.63469\times10^7$ | $1.13665\times10^6$ | $1.31473\times10^5$ | --[a] |
| 06CuAl-R | $5.18224\times10^7$ | $0.79961\times10^7$ | $3.04514\times10^6$ | $0.37276\times10^5$ | $1.13936\times10^5$ |
| 06CuAl-RO | $6.88297\times10^7$ | $1.82832\times10^7$ | $2.40441\times10^6$ | $0.80723\times10^5$ | $1.34768\times10^5$ |

[a] It is hard to integrate the peak area under the current conditions.

Fig. S3 presents the NO-TPD profiles of $NO_2$ and $O_2$ over 06CuAl catalysts with different valence states. All the catalysts exhibit three desorption peaks in $NO_2$ profiles (Fig. S3a), the low-temperature peak (about 100 °C) originates from the

reaction between the desorbed NO and oxygen atom (O) resulted from the dissociation of the adsorbed NO species, the two high-temperature peaks (above 350 °C) are related to the decomposition of the surface adsorbed nitrites and nitrates.[S6,S7] Interestingly, the $NO_2$ desorption peak area of 06CuAl-R and 06CuAl-RO catalysts is smaller than that of 06CuAl catalyst (Table S2), the possible reason is that the atomic oxygen (O) resulted from the dissociation of the adsorbed NO species is consumed by oxidizing the low-valence state copper species in 06CuAl-R and 06CuAl-RO catalysts, which inhibits the combination with the desorbed NO to form $NO_2$. The $O_2$ desorption peak of 06CuAl-R and 06CuAl-RO catalysts is very weak, compared with 06CuAl catalyst (Fig. S3b). It is well known that the oxygen atom (O) resulted from the dissociation of the adsorbed NO species can be consumed by oxidizing the reduced state catalyst or combining with the desorbed NO to generate $NO_2$. However, the $NO_2$ desorption peaks of 06CuAl-R and 06CuAl-RO catalysts are also weaker than those of 06CuAl catalyst. As a result, the oxygen atom (O) resulted from the dissociation of the adsorbed NO species is mainly consumed by oxidizing the low-valence state copper species in 06CuAl-R and 06CuAl-RO catalysts, which leads to the weak $O_2$ desorption peak. $NO_2$ and $O_2$ are not the desired products in the reaction of NO reduction by CO, the existence of them is not conducive to the reaction. Therefore, the ability of promoting this reaction can be ranked by $Cu^0 > Cu^+ > Cu^{2+}$.

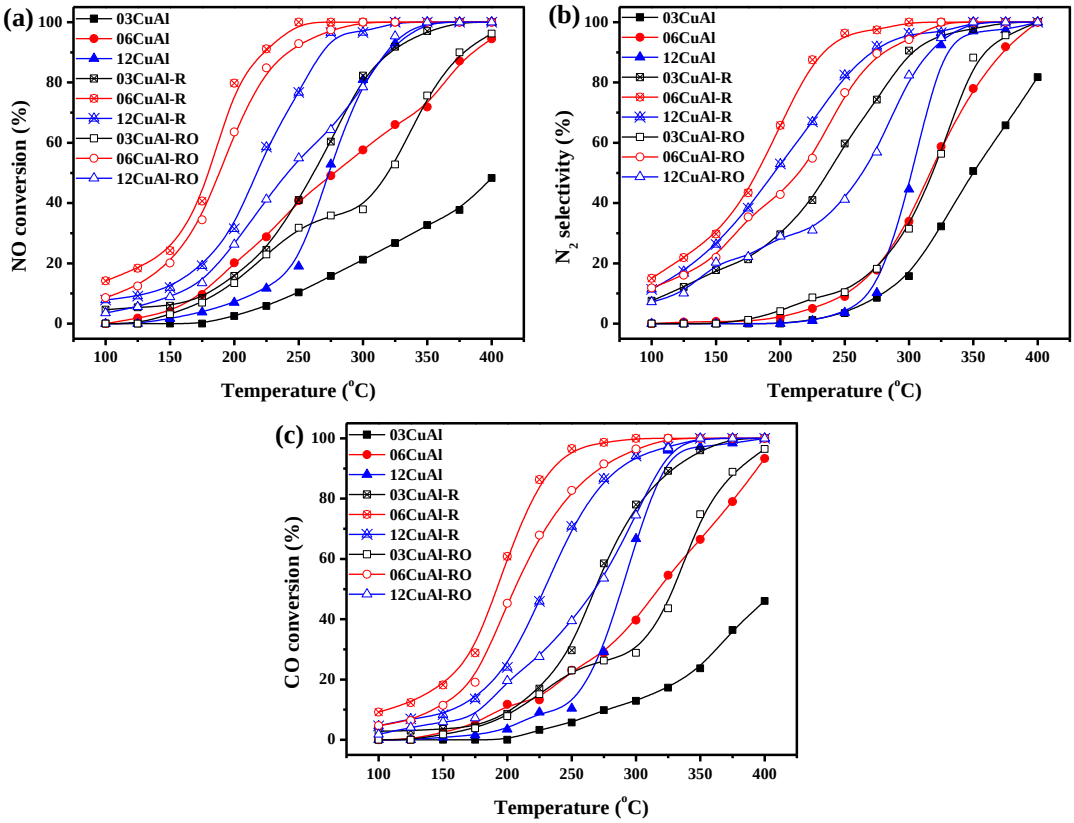


**Fig. S4** Catalytic performance of these *x*CuAl catalysts with different valence states as a function of reaction temperature: (a) NO conversion, (b) $N_2$ selectivity, and (c) CO conversion.

**Table S3** The light-off temperature of 50% NO and 50% CO conversion ($T_{50}$), as well as the turnover frequency (TOF) of NO and CO at 250 °C over these *x*CuAl catalysts with different valence states.

| Catalysts | $T_{50}$ [°C] | | TOF at 250 °C [$s^{-1} \times 10^{-3}$][a] | |
|---|---|---|---|---|
| | NO | CO | NO | CO |
| 03CuAl | >400 | >400 | 1.03 | 0.57 |
| 06CuAl | 278 | 317 | 2.09 | 1.18 |
| 12CuAl | 274 | 289 | 0.52 | 0.28 |
| 03CuAl-R | 261 | 268 | 4.08 | 2.96 |
| 06CuAl-R | 180 | 192 | 5.13 | 4.96 |
| 12CuAl-R | 214 | 229 | 2.09 | 1.93 |
| 03CuAl-RO | 320 | 329 | 3.17 | 2.29 |
| 06CuAl-RO | 188 | 205 | 4.77 | 4.25 |
| 12CuAl-RO | 242 | 268 | 1.50 | 1.07 |

[a] $TOF_{NO} = (P \cdot S_v \cdot C_{NO} \cdot X_{NO})/(R \cdot T \cdot n_{Cu})$, $TOF_{CO} = (P \cdot S_v \cdot C_{CO} \cdot X_{CO})/(R \cdot T \cdot n_{Cu})$, in which $P$ is the

atmospheric pressure ($1.013\times10^5$ Pa), $S_v$ is the space velocity (12,000 mL $g^{-1}$ $h^{-1}$), $C_{NO/CO}$ is the concentration of NO or CO at the inlet (NO: 5 mol.%, CO: 5 mol.%), $X_{NO/CO}$ is the NO or CO conversion, $R$ is the gas constant (8.314 J $K^{-1}$ $mol^{-1}$), $T$ is the reaction temperature in Kelvin units and $n_{Cu}$ is the molar number of Cu atoms.

**Table S4** The catalytic performance of the conventional supported noble-metal catalysts for NO reduction by CO reaction.

| Catalysts | space velocity ($h^{-1}$) | $T_{50}$ (°C) | | $T_{100}$ (°C)[a] | | References |
|---|---|---|---|---|---|---|
| | | NO | CO | NO | CO | |
| 06CuAl-R | 12,000 | 180 | 192 | 250 | 300 | This work |
| $Rh/Al_2O_3$ | 25,000 | 255 | 258 | 275 | 277 | S8 |
| $Pt\text{-}Rh/Al_2O_3$ | 25,000 | 306 | 310 | 320 | 370 | S8 |
| $Pt/ZrO_2$ | 120,000 | 412 | --[b] | 500 | -- | S9 |
| $Pt/ZrO_2\text{-}CeO_2\text{-}50$ | 120,000 | 371 | -- | 400 | -- | S9 |
| $Pt/ZrO_2\text{-}CeO_2\text{-}70$ | 120,000 | 365 | -- | 400 | -- | S9 |
| $Pt/CeO_2$ | 120,000 | 365 | -- | 400 | -- | S9 |
| $Pt/\alpha\text{-}Al_2O_3$ | 30,000 | 377 | -- | 430 | -- | S10 |
| $Pd/\alpha\text{-}Al_2O_3$ | 30,000 | 330 | -- | 375 | -- | S10 |
| $Pd/\alpha\text{-}Al_2O_3$ | 7,280 | 234 | -- | 254 | -- | S11 |
| $Pd/\alpha\text{-}Al_2O_3$ | 280,000 | 372 | -- | >400 | -- | S11 |
| $Pd/\gamma\text{-}Al_2O_3$ | 60,000 | 302 | -- | 402 | -- | S12 |
| $Pd/Al_2O_3/SiO_2$ | 50,000 | 251 | -- | 300 | -- | S13 |
| $Mo\text{-}Pd/Al_2O_3/SiO_2$ | 50,000 | 268 | -- | >300 | -- | S13 |
| $Pd/Al_2O_3$/Si-MCM-41 | 50,000 | 260 | -- | 300 | -- | S13 |
| $Mo\text{-}Pd/Al_2O_3$/Si-MCM-41 | 50,000 | 265 | -- | 300 | -- | S13 |

[a] The temperature of 100% NO and 100% CO conversion. [b] Not mentioned.

The catalytic performance for the simultaneous elimination of NO and CO over these *x*CuAl catalysts with different valence states is evaluated *via* NO reduction by CO reaction, and the corresponding results are exhibited in Fig. S4. For the fresh *x*CuAl samples, the catalytic performance enhances with the increase of copper oxide loading amount when it is lower than the dispersion capacity (0.75 mmol $Cu^{2+}$/100 $m^2$ $\gamma\text{-}Al_2O_3$), however, further increase of copper oxide loading amount exceeding the

dispersion capacity leads to the decline in the catalytic performance due to the formation of crystalline CuO, which is consistent with the results of XRD. Similar phenomena can be observed on the *x*CuAl-R and *x*CuAl-RO samples. Moreover, we can find that the catalytic performance for the simultaneous elimination of NO and CO can be ranked by *x*CuAl-R > *x*CuAl-RO > *x*CuAl for each copper oxide loading amount. Interestingly, $N_2$ selectivity of *x*CuAl-R catalysts is obviously higher than that of *x*CuAl-RO catalysts. The possible reason is that $N_2O$ can oxidize $Cu^0$ to form $Cu^+$, meanwhile, itself is reduced to $N_2$, which improves the $N_2$ selectivity. In order to clearly present the difference of catalytic performance among these *x*CuAl catalysts with different valence states, the light-off temperature of 50% NO conversion and 50% CO conversion ($T_{50}$), as well as the turnover frequency (TOF) of NO and CO per copper atom at 250 °C are summarized in Table S3. The obtained results suggest that the low-valence state copper species are beneficial to the enhancement of catalytic performance for the simultaneous elimination of NO and CO, and give a sequence of $Cu^0$ > $Cu^+$ > $Cu^{2+}$ for each copper oxide loading amount. Especially, the catalytic performance of 06CuAl-R catalyst can be comparable with that of conventional supported noble-metal catalysts (Table S4).

## References

S1 C. J. G. Van Der Grift, A. F. H. Wielers, B. P. J. Jogh, J. Van Beunum, M. De Boer, M. Versluijs-Helder and J. W. Geus, *J. Catal.*, 1991, **131**, 178-189.

S2 S. X. Xia, Z. L. Yuan, L. N. Wang, P. Chen and Z. Y. Hou, *Appl. Catal. A: Gen.*,

2011, **403**, 173-182.

S3 Z. L. Yuan, L. N. Wang, J. H. Wang, S. X. Xia, P. Chen, Z. Y. Hou and X. M. Zheng, *Appl. Catal. B: Environ.*, 2011, **101**, 431-440.

S4 H. Q. Wan, Z. Wang, J. Zhu, X. W. Li, B. Liu, F. Gao, L. Dong and Y. Chen, *Appl. Catal. B: Environ.*, 2008, **79**, 254-261.

S5 M. Yin, C. K. Wu, Y. B. Lou, C. Burda, J. T. Koberstein, Y. M. Zhu and S. O'Brien, *J. Am. Chem. Soc.*, 2005, **127**, 9506-9511.

S6 C. Torre-Abreu, C. Henriques, F. R. Ribeiro, G. Delahay and M. F. Ribeiro, *Catal. Today*, 1999, **54**, 407-418.

S7 D. Li, Q. Yu, S. S. Li, H. Q. Wan, L. J. Liu, L. Qi, B. Liu, F. Gao, L. Dong and Y. Chen, *Chem. Eur. J.*, 2011, **17**, 5668-5679.

S8 P. Granger, J. J. Lecomte, L. Leclercq and G. Leclercq, *Top. Catal.*, 2001, **16-17**, 349-354.

S9 R. Pérez-Hernández, F. Aguilar, A. Gómez-Cortés and G. Díaz, *Catal. Today*, 2005, **107-108**, 175-180.

S10 P. Bera, K. C. Patil, V. Jayaram, M. S. Hegde and G. N. Subbanna, *J. Mater. Chem.*, 1999, **9**, 1801-1806.

S11 A. M. Pisanu and C. E. Gigola, *Appl. Catal. B: Environ.*, 1999, **20**, 179-189.

S12 K. Almusaiteer and S. S. C. Chuang, *J. Catal.*, 1999, **184**, 189-201.

S13 J. M. D. Cónsul, I. Costilla, C. E. Gigola and I. M. Baibich, *Appl. Catal. A: Gen.*, 2008, **339**, 151-158.